Origin of Plasticity in Nanostructured Silicon

Zhidan Zeng,[1,*] Qiaoshi Zeng,[1,2] Mingyuan Ge,[3] Bin Chen,[1] Hongbo Lou,[1] Xiehang Chen,[1] Jinyuan Yan,[4] Wenge Yang,[1] Ho-kwang Mao,[1] Deren Yang,[5] and Wendy L. Mao[6,7]

[1]*Center for High Pressure Science and Technology Advanced Research, Pudong, Shanghai 201203, People's Republic of China*

[2]*Jiangsu Key Laboratory of Advanced Metallic Materials, School of Materials Science and Engineering, Southeast University, Nanjing 211189, People's Republic of China*

[3]*National Synchrotron Light Source II (NSLS-II), Brookhaven National Laboratory, Upton, New York 11973, USA*

[4]*Advanced Light Source, Lawrence Berkeley National Laboratory, Berkeley, California 94720, USA*

[5]*State Key Lab of Silicon Materials and School of Materials Science and Engineering, Zhejiang University, Hangzhou 310027, People's Republic of China*

[6]*Department of Geological Sciences, Stanford University, Stanford, California 94305, USA*

[7]*Stanford Institute for Materials and Energy Sciences, SLAC National Accelerator Laboratory, Menlo Park, California 94025, USA*

(Received 9 September 2019; revised manuscript received 30 March 2020; accepted 14 April 2020; published 7 May 2020)

The mechanism of plasticity in nanostructured Si has been intensively studied over the past decade but still remains elusive. Here, we used *in situ* high-pressure radial x-ray diffraction to simultaneously monitor the deformation and structural evolution of a large number of randomly oriented Si nanoparticles (SiNPs). In contrast to the high-pressure β-Sn phase dominated plasticity observed in large SiNPs (~100 nm), small SiNPs (~9 nm) display a high-pressure simple hexagonal phase dominated plasticity. Meanwhile, dislocation activity exists in all of the phases, but significantly weakens as the particle size decreases and only leads to subtle plasticity in the initial diamond cubic phase. Furthermore, texture simulations identify major active slip systems in all of the phases. These findings elucidate the origin of plasticity in nanostructured Si under stress and provide key guidance for the application of nanostructured Si.

DOI: 10.1103/PhysRevLett.124.185701

Plasticity is defined as the ability of a material to accommodate permanent deformation when the applied stress exceeds its yield strength, which prevents the catastrophic failure in materials. In brittle materials, the lack of intrinsic plasticity is a critical challenge when developing applications, and significant effort has been devoted to improving their plasticity [1,2]. The plastic deformation of coarse-grained crystalline materials is usually controlled by dislocations. For typical metals and alloys with nondirectional metallic bonding between atoms, the low-energy barrier for dislocation nucleation and motion results in excellent plasticity; whereas for materials with strong, directional covalent bonds such as Si, Ge, and most ceramics, the dislocation activity is suppressed, making them archetypal brittle materials. Interestingly, obvious plastic deformation has been observed in indentation experiments of bulk Si and Ge [3,4]. This emerging plasticity during mechanical loading is critical to the applications of Si [5]. The origin of the plasticity of Si has attracted extensive research interest [4,6,7]. For bulk Si, the indentation plasticity has been mainly attributed to the pressure-induced phase transition from the brittle diamond cubic phase (Si-I) to the ductile β-Sn phase (Si-II) under the high stress (pressure) during indentation, i.e., phase-transition-induced plasticity [4,6,7].

Because of the scaling down of Si integrated-circuit (IC) linewidths to a few nanometers and the widespread applications of nanostructured Si [8–10], it is critically important to understand the plasticity of Si at the nanoscale with domain sizes down to a few nanometers. This has proven quite challenging—in contrast to the well-known mechanism of plasticity in bulk Si, the response at the nanoscale has been the subject of much debate with regard to whether the plasticity is controlled by dislocations or by phase transitions [11–17]. For example, nanoindentation experiments on SiNPs suggest that the plastic deformation in large SiNPs (diameters of 67–169 nm) was associated with both phase transitions and dislocation gliding in the Si-I phase; whereas for smaller SiNPs in the "deconfinement" region (diameters of 19–57 nm), the plasticity is only driven by dislocations in the Si-I phase under extremely high stress (10–25 GPa), and phase transitions are believed to be suppressed [14]. Compression experiments on Si nanocubes (sizes of 20–65 nm) in a TEM also claimed leading partial dislocations in the Si-I phase are the dominant source of plasticity [11]. Meanwhile, in addition to dislocation gliding in the Si-I phase, phase transitions

 © 2020 American Physical Society

such as Si-I to Si-IV (a wurtzite phase) and Si-I to an amorphous phase were reported in compressed and/or indented Si nanopillars (diameter ~80 and ~150 nm) and nanowedges (width ~150 nm); and even dislocation-initiated amorphization was observed in tension experiments of Si nanowires (diameters below 70 nm) [13,15,16,18]. In addition to the experimental results, theoretical results also show disagreement. Molecular dynamics (MD) simulations using the Tersoff potential suggested the Si-I to Si-II phase transition initiates the plastic deformation during uniaxial compression of SiNPs with diameters up to 10 or 5–40 nm [12,17]. In contrast, dislocation-driven plasticity was observed in 5 and 10 nm SiNPs in another MD simulation using the Stillinger-Weber potential, in which phase transitions are absent [14].

The dramatic disagreement in experimental and theoretical results call for *in situ* experimental studies using reliable techniques with new capabilities. Since the plastic deformation of nanostructured Si requires high stress and may involve phase transitions, we used the *in situ* high-pressure radial x-ray diffraction (RXRD) to simultaneously monitor the elastic and plastic deformation as well as the crystal structural evolution of a large number of randomly orientated SiNPs with two representative sizes (large SiNPs with average diameters ~100 nm and small SiNPs ~9 nm) during compression (see Supplemental Material, Fig. S1 for more details of the samples [19]) [20]. This technique has been successfully used to investigate the elastic and plastic deformation in a variety of materials, including Ni nanoparticles, Fe, Zr, MgO, TiN, etc. [21–28]. In contrast to typical TEM studies that may introduce electron radiation effects and are limited in the number of samples that can be tested [29], our experiments use hard x rays and are based on the statistical behavior of a large number of SiNPs under the same experimental conditions. With quantitative data, our results show that the plastic deformation of SiNPs is dominated by pressure-induced phase transitions and the subsequent significant dislocation activity in the newly formed ductile high-pressure phase.

In situ high-pressure RXRD experiments on SiNPs were performed using panoramic diamond anvil cells (DACs) with a large opening angle in the radial direction, at beamline 12.2.2 of Advanced Light Source at Lawrence Berkeley National Laboratory, beamlines 16 ID-B and 13 ID-D (GSECARS) at the Advanced Photon Source, Argonne National Laboratory, and beamline 15U1, Shanghai Synchrotron Radiation Facility. The DAC was positioned with its compression axis perpendicular to the incident x-ray beam (see Supplemental Material, Fig. S2 [19]). Uniaxial compressive stress is imposed on the samples by the two opposed diamond anvils [30]. Samples were loaded into an x-ray transparent gasket without a pressure medium to introduce deviatoric stress. Two-dimensional (2D) diffraction images were collected on a MAR345 image plate or a MAR165 CCD detector (see Supplemental Material for details of the experimental implementation [19]).

Figure 1 shows the unrolled 2D diffraction images of the SiNPs during compression. For the large SiNPs [Fig. 1(a)], the Si-I phase starts to transform to the Si-II phase at ~8.3 GPa, lower than the transition pressure for the bulk Si (~12 GPa), mainly due to the high deviatoric stress in the RXRD experiment [31]. For the Si-I phase, the intensity along all the Debye rings is always quite uniform, implying nearly random crystallographic orientations of the particles. In contrast, the Si-II phase shows a strong preferred orientation (texture). For example, the (101) and (112) Debye rings of the Si-II phase show maximum intensity at azimuth angles of 0° and 180° (the axial direction, which is the direction with maximum compression) and minimum intensity at 90° and 270° (the direction with minimum compression), and vice versa for (200) and (220). During plastic deformation, dislocation gliding along slip systems

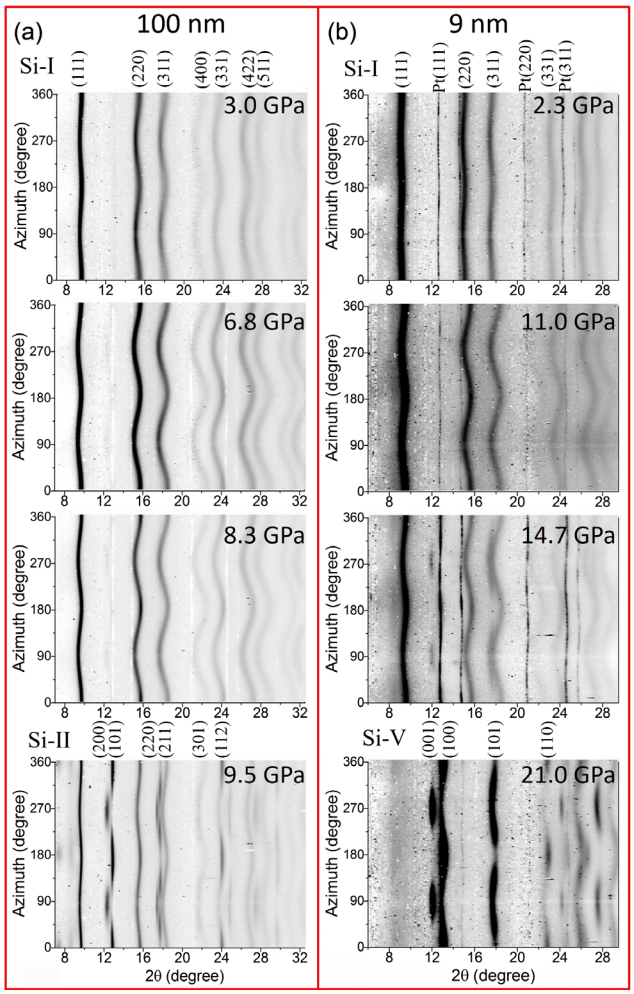

FIG. 1. 2D unrolled diffraction images of the (a) 100 nm SiNPs and (b) 9 nm SiNPs during compression. At the azimuth angle $\eta = 0°$ (360°) and 180° (along the DAC compression axis, maximum stress direction), the Debye-Scherrer rings shift to larger 2θ (smaller d spacing). The x-ray wavelength is 0.4959 Å.

usually results in a preferential crystallographic texture [32]. Therefore, the strong texture in the Si-II phase indicates extensive dislocation activities during compression, and consequently, considerable plastic deformation. This observation is consistent with the Si-II phase being a metallic phase with excellent plasticity [6]. The strong texture in the Si-II phase and the absence of pronounced texture in the initial Si-I phase imply that the high-pressure Si-II phase dominates the plastic deformation in relatively large SiNPs, similar to that in bulk Si [4,6].

For the small SiNPs [see Fig. 1(b)], the Si-I phase directly transforms into a simple hexagonal (Si-V) phase at ~14.7 GPa, rather than the Si-II or Si-IV phases claimed by previous TEM or simulation studies [12,13,17]. This transition is quite different from the sequence usually observed in compressed bulk Si, i.e., Si-I → Si-II → Si-XI → Si-V [31], but it is consistent with the transitions observed in Si nanocrystals with diameters of 3.2–4.5 nm using *in situ* high-pressure axial XRD [33]. In terms of texture, there is no obviously visible preferred orientation in the Si-I phase up to 14.7 GPa, whereas a strong texture is immediately present in the Si-V phase as soon as the phase transition occurs. These results suggest that during compression, extensive dislocation activities have occurred only in the Si-V phase. Therefore, the plasticity of small SiNPs down to sub-10 nm is dominated by the ductile Si-V phase, which is very different from the behavior of large SiNPs and bulk Si.

To further confirm the mechanism of plastic deformation in SiNPs, quantitative information was derived by analyzing and simulating the texture patterns. Each 2D diffraction image was integrated in 5° slices along the azimuth, and the XRD patterns obtained were then imported into the software package MAUD for Rietveld refinement and texture analysis, allowing detailed information of the texture development to be obtained [see Fig. 2(a) for an example refinement and the Supplemental Material for details [19]] [30]. Figure 2(b) shows the texture index of different Si phases as a function of pressure (the texture index is equal to 1 for a random distribution and increases with the degree of texture). Although not visible in Fig. 1, for large SiNPs, the texture index of the Si-I phase increases slightly during compression, indicating weak texture does emerge in Si-I and causes very limited plasticity when the stress is high enough. In contrast, the texture index of the Si-II phase reaches 3.8 multiples of a random distribution (mrd) at 8.3 GPa, demonstrating strong texture immediately built up in this phase once the Si-I to Si-II phase transition starts. For small SiNPs, the texture index of Si-I is almost constant below ~14.7 GPa and only shows very subtle change at ~14.7 GPa, while the texture index increases significantly when the Si-I phase transforms into the high-pressure Si-V phase. These results are generally consistent with the observation from the diffraction images in Fig. 1 and confirm that the plastic deformation in both large and small SiNPs is dominated by the intrinsic plasticity of the ductile high-pressure phases (Si-II or Si-V) rather than the very limited plasticity in the initial Si-I phase. For the Si-I phase, the obvious suppression of its texture development with decreasing particle size (from ~100 to ~9 nm) demonstrates that dislocation nucleation and/or motion is suppressed in small SiNPs. A similar phenomenon was observed in Ni nanoparticles since the critical resolved shear stress for dislocation nucleation is inversely proportional to the particle size [21,24,34]. Compared with the 100 nm SiNPs, the obviously weaker dislocation activities in the Si-I phase and the higher critical pressure for phase transitions in the 9 nm SiNPs could account for the high hardness and near-theoretical strength reported in small SiNPs [11,35].

Plastic deformation usually occurs after the strain in the material reaches its elastic limit, and the development of plastic deformation will be coupled with the release of the

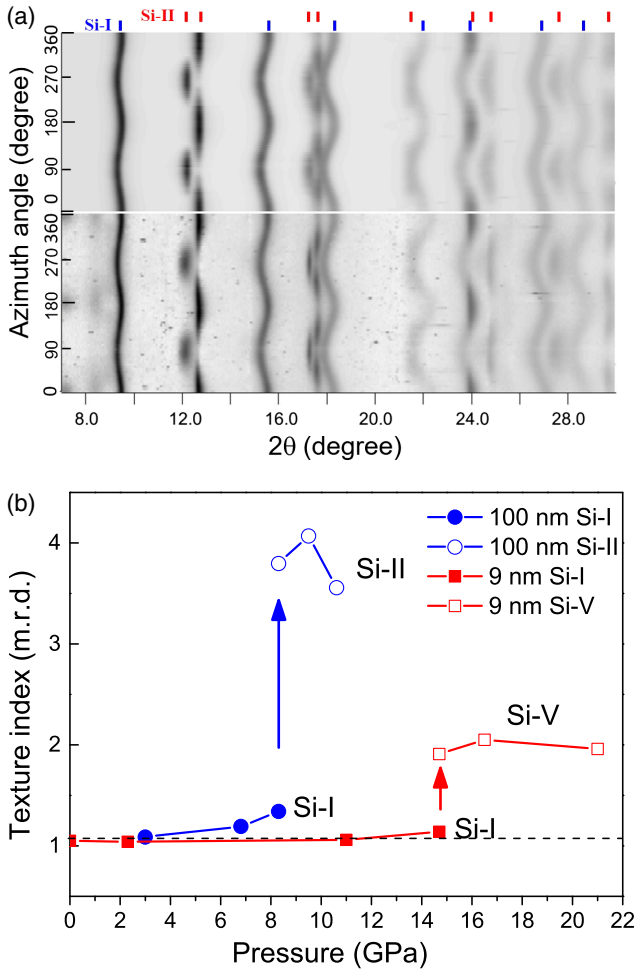

FIG. 2. (a) 2D unrolled image of 100 nm SiNPs at 9.5 GPa at which the Si-I and the Si-II phases coexist (bottom) and the corresponding Rietveld refinement result using MAUD (top). (b) Texture indexes of the Si-I (solid symbols), Si-II (open circles), and Si-V (open squares) phases as functions of pressure.

accumulated elastic strain. Therefore, the evolution of elastic strain in SiNPs during compression could also provide vital information to understand their plastic deformation. Figure 3(a) shows the d spacing of the Si-I (111) planes of the small SiNPs as a function of azimuth angle at different pressures, in which the periodic variation of d spacings is caused by the elastic lattice strain. Figure 3(b) presents the calculated lattice strain parameter (Q) for the Si-I (111) planes as a function of pressure (see Supplemental Material for details on the calculation of Q values [19]) [36]. For both samples, Q increases quickly with applied pressure at the beginning. As soon as the phase transition starts (Si-I to Si-II for large SiNPs, or Si-V for small SiNPs), Q immediately and significantly deviates from the original trend and even decreases with further compression. In high-pressure RXRD experiments, Q usually increases with pressure until the material starts to yield, and consequently, the local elastic stress and strain relax due to the plastic flow [22,37]. In our experiments, the continuous increase in Q before phase transitions indicates that the Si-I phase mainly deforms elastically, without obvious plastic deformation to relax the local elastic strain. Once the phase transition starts, large plastic deformation occurs in the emerging Si-II or Si-V phase, resulting in a substantial decrease in the deviatoric stress and the elastic lattice strain in the Si-I phase. These results further support that the ductile high-pressure phases (Si-II and Si-V) dominate the plastic deformation in SiNPs. It should be noted that once the phase transition occurs, the stress-strain relationship of the sample would change dramatically due to the coexistence of two phases (Si-I and Si-II, or Si-I and Si-V) with quite different mechanical properties, such as elastic moduli and yield strength. It is usually difficult to resolve the deformation behavior of one specific phase using conventional techniques. In this study, RXRD enables continuous monitoring of the development of the elastic strain in each phase during phase transitions.

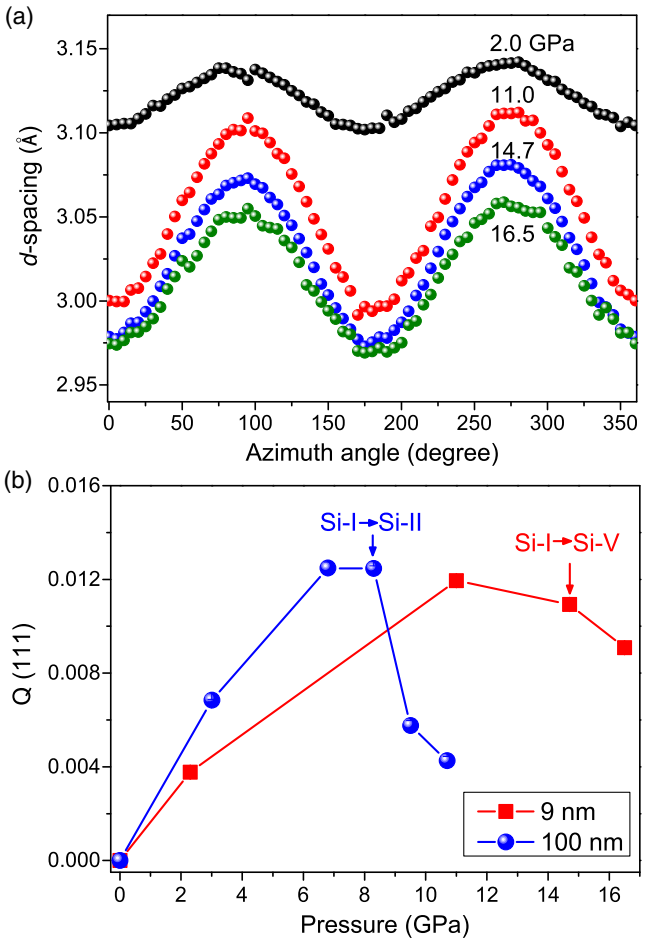

FIG. 3. (a) The d spacing of the Si-I (111) planes of the 9 nm SiNPs as a function of azimuth angle at different pressures. (b) Lattice strain parameter (Q) of the Si-I (111) plane as a function of pressure for large (100 nm) and small (9 nm) SiNPs. The arrows mark the pressure where the phase transition starts.

To elucidate the detailed mechanism at the atomic level of how these Si phases (Si-I, Si-II, and Si-V) deform, the inverse pole figures (IPFs), which describe the orientation of the compression axis relative to the crystalline coordinates, are derived for each phase as shown in Figs. 4(a)–(c) [38]. For the Si-I and the Si-II phases that coexisted at 9.5 GPa in large SiNPs, the maximum pole distribution is located near (011) in the Si-I phase and

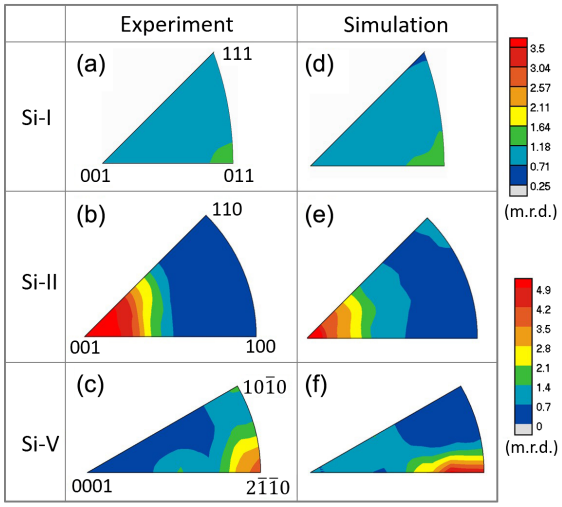

FIG. 4. Selected experimental inverse pole figures for the (a) Si-I, (b) Si-II (large SiNPs at 9.5 GPa), and (c) Si-V (small SiNPs at 14.7 GPa) phases along the compression direction (normal direction). The corresponding simulation results for the (d) Si-I, (e) Si-II, and (f) Si-V phases obtained from VPSC are shown in the right column. Because of different crystalline symmetry, different portions of the IPFs are needed to represent the orientation distribution for Si-I (a half quadrant), Si-II (45°), and Si-V (30°) phases. The pole densities are displayed on a color scale. The top color scale is for Si-I and the bottom scale is for Si-II and Si-V. Equal area projection and a linear scale are used. For the VPSC simulation, the strain was set to 4% for Si-I and 30% for both the Si-II and Si-V phases.

near (001) in the Si-II phase [see Figs. 4(a) and 4(b)]. For the Si-V phase in small SiNPs, the maximum pole distribution is located near $(2\bar{1}\,\bar{1}\,0)$ [see Fig. 4(c)]. It should be noted that both the Si-II and the Si-V phases cannot be recovered to ambient pressure; upon decompression, mainly Si-III phase (space group: $Ia\bar{3}$) and amorphous Si were obtained in the large and small SiNPs, respectively. Thus, the texture in the Si-II and the Si-V phases can only be observed by *in situ* high-pressure experiments.

Furthermore, the viscoplastic self-consistent (VPSC) code was used to simulate the texture formation in these Si phases based on the dislocation slip mechanism (see Supplemental Material for details of the simulations [19]) [39]. The simulation results were compared with the experimental data in Fig. 4, which match each other well. Based on our simulations, the slip system $\{111\}\langle\bar{1}10\rangle$ accounts for the texture observed in the Si-I phase in large SiNPs. This slip system is frequently observed in bulk Si-I deformed at elevated temperatures or in compressed Si nanopillars under high stress and confining pressure at room temperature [13,40]. Our results suggest this slip system can still be activated in 100 nm SiNPs at room temperature under high stress. The texture observed in the Si-II phase can be well reproduced by a combination of $\{001\}\langle100\rangle$ and $\{101\}\langle\bar{1}01\rangle$ slip systems. For the Si-V phase, the pole density maximum can be explained by the deformation through prismatic $\{10\bar{1}0\}\langle\bar{1}2\bar{1}0\rangle$ and pyramidal $\{10\bar{1}1\}\langle\bar{1}\,\bar{1}\,23\rangle$ slip systems.

In summary, the plastic and elastic deformation and structural evolution of SiNPs during compression were quantitatively investigated using *in situ* high-pressure RXRD. A new plasticity mechanism, the Si-I to Si-V phase transition dominated plasticity, was observed in compressed small SiNPs (~9 nm) in contrast to the Si-I to Si-II phase transition dominated plasticity in large SiNPs (~100 nm). The critical pressure for the former transition is ~14.7 GPa, while it is ~8.3 GPa for the latter transition. The absence of the high-pressure phases in some of the previous experiments on nanostructured Si could be attributed to the limited hydrostatic stress achieved. The plastic deformation driven by dislocation activities in the initial Si-I phase of SiNPs is extremely weak and becomes almost negligible when the size decreases down to ~9 nm, while pressure-induced phase transitions could result in large plasticity due to the density difference between different phases and the subsequent substantial dislocation nucleation and motions in the ductile high-pressure phases (Si-V or Si-II). The active slip systems of the Si-V or Si-II phase were revealed by texture simulations. These results demonstrate that complex plasticity mechanisms are involved during compression of SiNPs, quantitative methods are needed to determine the real dominant factor. By clarifying the atomic mechanism of plasticity in SiNPs, this Letter can help to guide the design of various nanostructured Si-based devices and also could shed light on the deformation behavior of similar covalent nanocrystals.

The authors thank Dr. Haini Dong for helpful discussion. The authors acknowledge financial support from the National Natural Science Foundation of China (U1930401, 51871054). Part of the XRD experiments was performed at the beamline 12.2.2, Advanced Light Source (ALS). ALS is supported by the Director, Office of Science, DOE-BES under Contract No. DE-AC02-05CH11231. Part of the XRD work was performed at beamlines 13 ID-D of GSECARS, 16 ID-B of HPCAT, Advanced Photon Source (APS), Argonne National Laboratory (ANL), and 15U1 of Shanghai Synchrotron Radiation Facility (SSRF), China. GSECARS is supported by NSF (EAR-1634415) and DOE (DE-FG02-94ER14466). HPCAT is supported by the Department of Energy (DOE)-National Nuclear Security Administration (NNSA) under Award No. DE-NA0001974 with partial instrumentation funding by the NSF. APS is supported by DOE, Office of Basic Energy Sciences (BES), under Contract No. DE-AC02-06CH11357.

*Corresponding author.
zengzd@hpstar.ac.cn

[1] B. R. Lawn, N. P. Padture, H. Cait, and F. Guiberteau, Making ceramics "Ductile", Science **263**, 1114 (1994).
[2] C. C. Hays, C. P. Kim, and W. L. Johnson, Microstructure Controlled Shear Band Pattern Formation and Enhanced Plasticity of Bulk Metallic Glasses Containing in situ Formed Ductile Phase Dendrite Dispersions, Phys. Rev. Lett. **84**, 2901 (2000).
[3] A. P. Gerk and D. Tabor, Indentation hardness and semiconductor–metal transition of germanium and silicon, Nature (London) **271**, 732 (1978).
[4] G. M. Pharr, W. C. Oliver, and D. R. Clarke, The mechanical behavior of silicon during small-scale indentation, J. Electron. Mater. **19**, 881 (1990).
[5] P. N. Blake and R. O. Scattergood, Ductile-regime machining of germanium and silicon, J. Am. Ceram. Soc. **73**, 949 (1990).
[6] R. W. Cahn, Metallic solid silicon, Nature (London) **357**, 645 (1992).
[7] R. Abram, D. Chrobak, and R. Nowak, Origin of a Nanoindentation Pop-in Event in Silicon Crystal, Phys. Rev. Lett. **118**, 095502 (2017).
[8] C. K. Chan, H. Peng, G. Liu, K. McIlwrath, X. F. Zhang, R. A. Huggins, and Y. Cui, High-performance lithium battery anodes using silicon nanowires, Nat. Nanotechnol. **3**, 31 (2008).
[9] Z. Zeng, Q. Zeng, N. Liu, A. R. Oganov, Q. Zeng, Y. Cui, and W. L. Mao, A novel phase of $Li_{15}Si_4$ synthesized under pressure, Adv. Energy Mater. **5**, 1500214 (2015).
[10] H. G. Craighead, Nanoelectromechanical systems, Science **290**, 1532 (2000).
[11] A. J. Wagner, E. D. Hintsala, P. Kumar, W. W. Gerberich, and K. A. Mkhoyan, Mechanisms of plasticity in

near-theoretical strength sub-100 nm Si nanocubes, Acta Mater. **100**, 256 (2015).
[12] N. Zhang *et al.*, Deformation mechanisms in silicon nanoparticles, J. Appl. Phys. **109**, 063534 (2011).
[13] Y. He, L. Zhong, F. Fan, C. Wang, T. Zhu, and S. X. Mao, In situ observation of shear-driven amorphization in silicon crystals, Nat. Nanotechnol. **11**, 866 (2016).
[14] D. Chrobak, N. Tymiak, A. Beaber, O. Ugurlu, W. W. Gerberich, and R. Nowak, Deconfinement leads to changes in the nanoscale plasticity of silicon, Nat. Nanotechnol. **6**, 480 (2011).
[15] Y.-C. Wang, W. Zhang, L.-Y. Wang, Z. Zhuang, E. Ma, J. Li, and Z.-W. Shan, In situ TEM study of deformation-induced crystalline-to-amorphous transition in silicon, NPG Asia Mater. **8**, e291 (2016).
[16] A. M. Minor, E. T. Lilleodden, M. Jin, E. A. Stach, D. C. Chrzan, and J. W. Morris, Room temperature dislocation plasticity in silicon, Philos. Mag. **85**, 323 (2005).
[17] P. Valentini, W. W. Gerberich, and T. Dumitrica, Phase-Transition Plasticity Response in Uniaxially Compressed Silicon Nanospheres, Phys. Rev. Lett. **99**, 175701 (2007).
[18] X. Han, K. Zheng, Y. Zhang, X. Zhang, Z. Zhang, and Z. L. Wang, Low-temperature in situ large-strain plasticity of silicon nanowires, Adv. Mater. **19**, 2112 (2007).
[19] See Supplemental Material at http://link.aps.org/supplemental/10.1103/PhysRevLett.124.185701 for detailed description of high-pressure RXRD experiments, data analysis method, and VPSC simulations, as well as TEM images of the SiNPs, a schematic diagram of the experimental setup, and an example of linear fitting that gives the elastic lattice strain (Q), which includes Ref. [20].
[20] D. Bahattin and A. Işik, Investigation of operative slip system in β-sn single crystal and the relation between the crystal orientation and the slip systems, Jpn. J. Appl. Phys. **32**, 3214 (1993).
[21] B. Chen *et al.*, Texture of nanocrystalline nickel: probing the lower size limit of dislocation activity, Science **338**, 1448 (2012).
[22] H. Chen, F. Peng, H.-k. Mao, G. Shen, H.-P. Liermann, Z. Li, and J. Shu, Strength and elastic moduli of TiN from radial x-ray diffraction under nonhydrostatic compression up to 45 GPa, J. Appl. Phys. **107**, 113503 (2010).
[23] S. Merkel, H. R. Wenk, J. Shu, G. Shen, P. Gillet, H.-k. Mao, and R. J. Hemley, Deformation of polycrystalline MgO at pressures of the lower mantle, J. Geophys. Res. Solid Earth **107**, ECV 3-1 (2002).
[24] X. Zhou *et al.*, High-pressure strengthening in ultrafine-grained metals, Nature (London) **579**, 67 (2020).
[25] H. R. Wenk, S. Matthies, R. J. Hemley, H. K. Mao, and J. Shu, The plastic deformation of iron at pressures of the Earth's inner core, Nature (London) **405**, 1044 (2000).
[26] S. Merkel, A. Kubo, L. Miyagi, S. Speziale, T. S. Duffy, H.-k. Mao, and H.-R. Wenk, Plastic Deformation of $MgGeO_3$ Post-Perovskite at Lower Mantle Pressures, Science **311**, 644 (2006).
[27] H. R. Wenk, P. Kaercher, W. Kanitpanyacharoen, E. Zepeda-Alarcon, and Y. Wang, Orientation Relations During the α-ω Phase Transition of Zirconium: In Situ Texture Observations at High Pressure and Temperature, Phys. Rev. Lett. **111**, 195701 (2013).
[28] H.-K. Mao, B. Chen, J. Chen, K. Li, J.-F. Lin, W. Yang, and H. Zheng, Recent advances in high-pressure science and technology, Matter Radiat. Extremes **1**, 59 (2016).
[29] K. Zheng *et al.*, Electron-beam-assisted superplastic shaping of nanoscale amorphous silica, Nat. Commun. **1**, 24 (2010).
[30] H.-R. Wenk, L. Lutterotti, P. Kaercher, W. Kanitpanyacharoen, L. Miyagi, and R. Vasin, Rietveld texture analysis from synchrotron diffraction images. II. Complex multiphase materials and diamond anvil cell experiments, Powder Diffr. **29**, 220 (2014).
[31] A. Mujica, A. Rubio, A. Munoz, and R. J. Needs, High-pressure phases of group-IV, III–V, and II–VI compounds, Rev. Mod. Phys. **75**, 863 (2003).
[32] S. Suwas and R. K. Ray, *Crystallographic Texture of Materials* (Springer, London, 2014), pp. 95–98.
[33] D. C. Hannah, J. Yang, P. Podsiadlo, M. K. Y. Chan, A. Demortière, D. J. Gosztola, V. B. Prakapenka, G. C. Schatz, U. Kortshagen, and R. D. Schaller, On the origin of photoluminescence in silicon nanocrystals: pressure-dependent structural and optical studies, Nano Lett. **12**, 4200 (2012).
[34] Z. Shan, E. A. Stach, J. M. K. Wiezorek, J. A. Knapp, D. M. Follstaedt, and S. X. Mao, Grain boundary-mediated plasticity in nanocrystalline nickel, Science **305**, 654 (2004).
[35] W. W. Gerberich, W. M. Mook, C. R. Perrey, C. B. Carter, M. I. Baskes, R. Mukherjee, A. Gidwani, J. Heberlein, P. H. McMurry, and S. L. Girshick, Superhard silicon nanospheres, J. Mech. Phys. Solids **51**, 979 (2003).
[36] A. K. Singh, The lattice strain in a specimen (cubic system) compressed nonhydrostatically in an opposed anvil device, J. Appl. Phys. **73**, 4278 (1993).
[37] D. He, S. R. Shieh, and T. S. Duffy, Strength and equation of state of boron suboxide from radial x-ray diffraction in a diamond cell under nonhydrostatic compression, Phys. Rev. B **70**, 184121 (2004).
[38] H.-R. Wenk, S. Matthies, J. Donovan, and D. Chateigner, BEARTEX: a Windows-based program system for quantitative texture analysis, J. Appl. Crystallogr. **31**, 262 (1998).
[39] R. A. Lebensohn and C. N. Tomé, A self-consistent anisotropic approach for the simulation of plastic deformation and texture development of polycrystals: Application to zirconium alloys, Acta Metal. Mater. **41**, 2611 (1993).
[40] J. Rabier, L. Pizzagalli, and J. L. Demenet, in *Dislocations in Solids*, edited by J. P. Hirth and L. Kubin (Elsevier, New York, 2010), p. 47.